

Proceedings of the 12th International Conference on
Computational Fluid Dynamics in the Oil & Gas,
Metallurgical and Process Industries

Progress in Applied CFD – CFD2017



SINTEF Proceedings

Editors:

Jan Erik Olsen and Stein Tore Johansen

Progress in Applied CFD – CFD2017

Proceedings of the 12th International Conference on Computational Fluid Dynamics
in the Oil & Gas, Metallurgical and Process Industries

SINTEF Academic Press

SINTEF Proceedings no 2

Editors: Jan Erik Olsen and Stein Tore Johansen

Progress in Applied CFD – CFD2017

Selected papers from 10th International Conference on Computational Fluid Dynamics in the Oil & Gas, Metallurgical and Process Industries

Key words:

CFD, Flow, Modelling

Cover, illustration: Arun Kamath

ISSN 2387-4295 (online)

ISBN 978-82-536-1544-8 (pdf)

© Copyright SINTEF Academic Press 2017

The material in this publication is covered by the provisions of the Norwegian Copyright Act. Without any special agreement with SINTEF Academic Press, any copying and making available of the material is only allowed to the extent that this is permitted by law or allowed through an agreement with Kopinor, the Reproduction Rights Organisation for Norway. Any use contrary to legislation or an agreement may lead to a liability for damages and confiscation, and may be punished by fines or imprisonment

SINTEF Academic Press

Address: Forskningsveien 3 B
 PO Box 124 Blindern
 N-0314 OSLO

Tel: +47 73 59 30 00

Fax: +47 22 96 55 08

www.sintef.no/byggforsk

www.sintefbok.no

SINTEF Proceedings

SINTEF Proceedings is a serial publication for peer-reviewed conference proceedings on a variety of scientific topics.

The processes of peer-reviewing of papers published in SINTEF Proceedings are administered by the conference organizers and proceedings editors. Detailed procedures will vary according to custom and practice in each scientific community.

PREFACE

This book contains all manuscripts approved by the reviewers and the organizing committee of the 12th International Conference on Computational Fluid Dynamics in the Oil & Gas, Metallurgical and Process Industries. The conference was hosted by SINTEF in Trondheim in May/June 2017 and is also known as CFD2017 for short. The conference series was initiated by CSIRO and Phil Schwarz in 1997. So far the conference has been alternating between CSIRO in Melbourne and SINTEF in Trondheim. The conferences focuses on the application of CFD in the oil and gas industries, metal production, mineral processing, power generation, chemicals and other process industries. In addition pragmatic modelling concepts and bio-mechanical applications have become an important part of the conference. The papers in this book demonstrate the current progress in applied CFD.

The conference papers undergo a review process involving two experts. Only papers accepted by the reviewers are included in the proceedings. 108 contributions were presented at the conference together with six keynote presentations. A majority of these contributions are presented by their manuscript in this collection (a few were granted to present without an accompanying manuscript).

The organizing committee would like to thank everyone who has helped with review of manuscripts, all those who helped to promote the conference and all authors who have submitted scientific contributions. We are also grateful for the support from the conference sponsors: ANSYS, SFI Metal Production and NanoSim.

Stein Tore Johansen & Jan Erik Olsen



Organizing committee:

Conference chairman: Prof. Stein Tore Johansen

Conference coordinator: Dr. Jan Erik Olsen

Dr. Bernhard Müller

Dr. Sigrid Karstad Dahl

Dr. Shahriar Amini

Dr. Ernst Meese

Dr. Josip Zoric

Dr. Jannike Solsvik

Dr. Peter Witt

Scientific committee:

Stein Tore Johansen, SINTEF/NTNU

Bernhard Müller, NTNU

Phil Schwarz, CSIRO

Akio Tomiyama, Kobe University

Hans Kuipers, Eindhoven University of Technology

Jinghai Li, Chinese Academy of Science

Markus Braun, Ansys

Simon Lo, CD-adapco

Patrick Segers, Universiteit Gent

Jiyuan Tu, RMIT

Jos Derksen, University of Aberdeen

Dmitry Eskin, Schlumberger-Doll Research

Pär Jönsson, KTH

Stefan Pirker, Johannes Kepler University

Josip Zoric, SINTEF

CONTENTS

PRAGMATIC MODELLING	9
On pragmatism in industrial modeling. Part III: Application to operational drilling	11
CFD modeling of dynamic emulsion stability	23
Modelling of interaction between turbines and terrain wakes using pragmatic approach	29
FLUIDIZED BED	37
Simulation of chemical looping combustion process in a double looping fluidized bed reactor with cu-based oxygen carriers.....	39
Extremely fast simulations of heat transfer in fluidized beds.....	47
Mass transfer phenomena in fluidized beds with horizontally immersed membranes	53
A Two-Fluid model study of hydrogen production via water gas shift in fluidized bed membrane reactors	63
Effect of lift force on dense gas-fluidized beds of non-spherical particles	71
Experimental and numerical investigation of a bubbling dense gas-solid fluidized bed	81
Direct numerical simulation of the effective drag in gas-liquid-solid systems	89
A Lagrangian-Eulerian hybrid model for the simulation of direct reduction of iron ore in fluidized beds.....	97
High temperature fluidization - influence of inter-particle forces on fluidization behavior	107
Verification of filtered two fluid models for reactive gas-solid flows	115
BIOMECHANICS.....	123
A computational framework involving CFD and data mining tools for analyzing disease in carotid artery	125
Investigating the numerical parameter space for a stenosed patient-specific internal carotid artery model.....	133
Velocity profiles in a 2D model of the left ventricular outflow tract, pathological case study using PIV and CFD modeling.....	139
Oscillatory flow and mass transport in a coronary artery.....	147
Patient specific numerical simulation of flow in the human upper airways for assessing the effect of nasal surgery.....	153
CFD simulations of turbulent flow in the human upper airways	163
OIL & GAS APPLICATIONS	169
Estimation of flow rates and parameters in two-phase stratified and slug flow by an ensemble Kalman filter	171
Direct numerical simulation of proppant transport in a narrow channel for hydraulic fracturing application	179
Multiphase direct numerical simulations (DNS) of oil-water flows through homogeneous porous rocks	185
CFD erosion modelling of blind tees	191
Shape factors inclusion in a one-dimensional, transient two-fluid model for stratified and slug flow simulations in pipes	201
Gas-liquid two-phase flow behavior in terrain-inclined pipelines for wet natural gas transportation	207

NUMERICS, METHODS & CODE DEVELOPMENT	213
Innovative computing for industrially-relevant multiphase flows	215
Development of GPU parallel multiphase flow solver for turbulent slurry flows in cyclone.....	223
Immersed boundary method for the compressible Navier–Stokes equations using high order summation-by-parts difference operators	233
Direct numerical simulation of coupled heat and mass transfer in fluid-solid systems	243
A simulation concept for generic simulation of multi-material flow, using staggered Cartesian grids.....	253
A cartesian cut-cell method, based on formal volume averaging of mass, momentum equations.....	265
SOFT: a framework for semantic interoperability of scientific software	273
 POPULATION BALANCE	 279
Combined multifluid-population balance method for polydisperse multiphase flows	281
A multifluid-PBE model for a slurry bubble column with bubble size dependent velocity, weight fractions and temperature.....	285
CFD simulation of the droplet size distribution of liquid-liquid emulsions in stirred tank reactors	295
Towards a CFD model for boiling flows: validation of QMOM predictions with TOPFLOW experiments	301
Numerical simulations of turbulent liquid-liquid dispersions with quadrature-based moment methods.....	309
Simulation of dispersion of immiscible fluids in a turbulent couette flow	317
Simulation of gas-liquid flows in separators - a Lagrangian approach.....	325
CFD modelling to predict mass transfer in pulsed sieve plate extraction columns	335
 BREAKUP & COALESCENCE	 343
Experimental and numerical study on single droplet breakage in turbulent flow	345
Improved collision modelling for liquid metal droplets in a copper slag cleaning process	355
Modelling of bubble dynamics in slag during its hot stage engineering.....	365
Controlled coalescence with local front reconstruction method	373
 BUBBLY FLOWS	 381
Modelling of fluid dynamics, mass transfer and chemical reaction in bubbly flows	383
Stochastic DSMC model for large scale dense bubbly flows.....	391
On the surfacing mechanism of bubble plumes from subsea gas release.....	399
Bubble generated turbulence in two fluid simulation of bubbly flow	405
 HEAT TRANSFER	 413
CFD-simulation of boiling in a heated pipe including flow pattern transitions using a multi-field concept	415
The pear-shaped fate of an ice melting front	423
Flow dynamics studies for flexible operation of continuous casters (flow flex cc).....	431
An Euler-Euler model for gas-liquid flows in a coil wound heat exchanger.....	441
 NON-NEWTONIAN FLOWS.....	 449
Viscoelastic flow simulations in disordered porous media	451
Tire rubber extrudate swell simulation and verification with experiments	459
Front-tracking simulations of bubbles rising in non-Newtonian fluids.....	469
A 2D sediment bed morphodynamics model for turbulent, non-Newtonian, particle-loaded flows.....	479

METALLURGICAL APPLICATIONS.....	491
Experimental modelling of metallurgical processes	493
State of the art: macroscopic modelling approaches for the description of multiphysics phenomena within the electroslag remelting process	499
LES-VOF simulation of turbulent interfacial flow in the continuous casting mold	507
CFD-DEM modelling of blast furnace tapping	515
Multiphase flow modelling of furnace tapholes	521
Numerical predictions of the shape and size of the raceway zone in a blast furnace.....	531
Modelling and measurements in the aluminium industry - Where are the obstacles?	541
Modelling of chemical reactions in metallurgical processes.....	549
Using CFD analysis to optimise top submerged lance furnace geometries	555
Numerical analysis of the temperature distribution in a martensitic stainless steel strip during hardening.....	565
Validation of a rapid slag viscosity measurement by CFD.....	575
Solidification modeling with user defined function in ANSYS Fluent.....	583
Cleaning of polycyclic aromatic hydrocarbons (PAH) obtained from ferroalloys plant.....	587
Granular flow described by fictitious fluids: a suitable methodology for process simulations	593
A multiscale numerical approach of the dripping slag in the coke bed zone of a pilot scale Si-Mn furnace.....	599
INDUSTRIAL APPLICATIONS	605
Use of CFD as a design tool for a phosphoric acid plant cooling pond	607
Numerical evaluation of co-firing solid recovered fuel with petroleum coke in a cement rotary kiln: Influence of fuel moisture	613
Experimental and CFD investigation of fractal distributor on a novel plate and frame ion-exchanger	621
COMBUSTION	631
CFD modeling of a commercial-size circle-draft biomass gasifier.....	633
Numerical study of coal particle gasification up to Reynolds numbers of 1000.....	641
Modelling combustion of pulverized coal and alternative carbon materials in the blast furnace raceway	647
Combustion chamber scaling for energy recovery from furnace process gas: waste to value	657
PACKED BED.....	665
Comparison of particle-resolved direct numerical simulation and 1D modelling of catalytic reactions in a packed bed	667
Numerical investigation of particle types influence on packed bed adsorber behaviour	675
CFD based study of dense medium drum separation processes	683
A multi-domain 1D particle-reactor model for packed bed reactor applications.....	689
SPECIES TRANSPORT & INTERFACES	699
Modelling and numerical simulation of surface active species transport - reaction in welding processes	701
Multiscale approach to fully resolved boundary layers using adaptive grids.....	709
Implementation, demonstration and validation of a user-defined wall function for direct precipitation fouling in Ansys Fluent.....	717

FREE SURFACE FLOW & WAVES	727
Unresolved CFD-DEM in environmental engineering: submarine slope stability and other applications.....	729
Influence of the upstream cylinder and wave breaking point on the breaking wave forces on the downstream cylinder	735
Recent developments for the computation of the necessary submergence of pump intakes with free surfaces	743
Parallel multiphase flow software for solving the Navier-Stokes equations	752
 PARTICLE METHODS	 759
A numerical approach to model aggregate restructuring in shear flow using DEM in Lattice-Boltzmann simulations	761
Adaptive coarse-graining for large-scale DEM simulations.....	773
Novel efficient hybrid-DEM collision integration scheme.....	779
Implementing the kinetic theory of granular flows into the Lagrangian dense discrete phase model.....	785
Importance of the different fluid forces on particle dispersion in fluid phase resonance mixers	791
Large scale modelling of bubble formation and growth in a supersaturated liquid.....	798
 FUNDAMENTAL FLUID DYNAMICS	 807
Flow past a yawed cylinder of finite length using a fictitious domain method	809
A numerical evaluation of the effect of the electro-magnetic force on bubble flow in aluminium smelting process.....	819
A DNS study of droplet spreading and penetration on a porous medium.....	825
From linear to nonlinear: Transient growth in confined magnetohydrodynamic flows.....	831

BUBBLE GENERATED TURBULENCE IN TWO FLUID SIMULATION OF BUBBLY FLOW

M. Philip SCHWARZ^{1*}, Yuqing Feng¹, Peter J. Witt¹

¹ CSIRO Minerals Resources, Clayton, AUSTRALIA

* E-mail: phil.schwarz@csiro.au

ABSTRACT

Bubbly flows are central to many processes in the minerals extraction and metal production industries, mainly because they enhance heat and mass transfer rates. These transfer rates depend on the turbulence level in the multiphase flow. Bubbles rising in a liquid give rise to an additional component of turbulence in the continuous phase, known as bubble-induced turbulence. Various models have been proposed in the literature to account for this mechanism in two-fluid Reynolds-averaged (RANS) simulations of bubbly flow, but there is considerable uncertainty about the form of terms that should be added to account for the effect, and even the flow physics underlying the phenomenon is poorly understood. Simulations are carried out of flow around a simplified bubble arrangement in order to clarify this flow physics, to allow a consistent definition of bubble-induced turbulence, and to point the way to a reliable determination of the source terms. It is argued that a component of the fluctuations due to flow around bubbles should not be considered to be turbulence since the energy of these fluctuations is actually recoverable. This fact seriously complicates efforts to obtain bubble-induced turbulence from experimental velocity measurements or direct numerical simulations. Simulations of flow around a bubble using the SST turbulence model allow the prediction of the source of actual bubble-induced turbulence for a single isolated rather than the pseudo-turbulence related to bubble motion. The source of actual turbulence for an isolated bubble of diameter 5 mm with a mobile interface is predicted to be very small, while for an immobile interface, a finite source is distributed in the wake of the bubble. The source of “bubble-induced” turbulence for a bubble swarm is a more complex issue, but the present simulations can give insights and point the way forward to a more complete formulation.

Keywords: Multiphase flow, bubble induced turbulence, two fluid simulation, turbulence kinetic energy, CFD.

NOMENCLATURE

Greek Symbols

- α Volume fraction, [-].
- ε Dissipation rate of turbulence energy, [m^2/s^3].
- κ Empirical constant, [-].
- ν Kinematic viscosity, [$\text{kg}/\text{m}\cdot\text{s}$].
- ρ Mass density, [kg/m^3].
- μ Dynamic viscosity, [$\text{kg}/\text{m}\cdot\text{s}$].

τ Total shear stress, [$\text{kg}/\text{m}\cdot\text{s}^2$].

Latin Symbols

- b_2 Coefficient, [-].
- c_2 Coefficient, [-].
- C_d Drag coefficient, [-].
- C_{vm} Virtual mass coefficient, [-].
- d_b Bubble diameter, [m].
- k Kinetic energy of turbulence, [m^2/s^2].
- p Pressure, [Pa].
- \mathbf{T} Tensor stress, [$\text{kg}/\text{m}\cdot\text{s}^2$].
- U_b Bubble slip velocity, [m/s].
- U Velocity, [m/s].
- y Coordinate perpendicular to velocity, [m].

Sub/superscripts

- BI Bubble induced.
- BIT Bubble induced turbulence.
- g Gas.
- l Liquid.
- t Turbulent.

INTRODUCTION

Many processes in the chemicals and mineral processing industries involve injection of bubbles into a liquid, either as a direct reagent or to induce flow and mixing. Examples include bubble columns, three-phase fluidized beds, mineral flotation cells, some intensive smelting processes, as well as numerous specialized processes such as ladle refining, aluminium smelting, and so on. Computational Fluid Dynamics (CFD) modelling is a powerful tool to assist design and optimisation of such processes, but the complexity of the multi-scale flow involved means that approximations involving ‘modelling’ of micro- and meso-scale phenomena are required in order to simulate large-scale industrial systems (Schwarz and Feng, 2015).

In large-scale chemical and mineral reactors of the sort mentioned above, heat and mass transfer phenomena are usually central to the process operation. Bubbles can play a critical role here, both in participating directly through chemical reactions, and also by stirring the liquid. For example, in bubble columns and mineral flotation columns, the buoyancy of bubbles results in large-scale mixing within the reactor. At the same time, bubbles cause mixing at a wide range of length scales in such reactors, leading to local enhancement of heat and mass transfer rates, as well as overall mixing. So the ability to design and control the bubble flow and the associated transfer phenomena is crucial to the successful operation of such a process. This is the reason there has been an increasing trend of applying detailed multi-dimensional CFD modelling of the two-phase flow as a design tool.

The typical number of bubbles in large-scale reactors such as bubble columns and flotation cells is huge, so that direct simulation of the full detail of all bubble–liquid interactions is still not computationally feasible. For this reason, techniques have been developed in which the Navier-Stokes equations are averaged over fluctuations associated with individual bubbles. In this way, separate averaged equations are obtained for the liquid and gas phases, and for this reason, the approach is known as the multi-fluid model, (see, for example, Spalding, 1981). The gas and liquid velocity equations are coupled through interaction terms, that can in principle be determined as part of the averaging process. In practice, the flow interactions are usually so complex that theory and empiricism must be used to define and evaluate the interaction terms. The primary interaction term is of course drag, but there are several others such as the so-called lift force.

Bubbly flow in large-scale reactors is almost invariably turbulent. Because of the large scale and physico-chemical complexity, industrial simulations still treat turbulence in the flow using Reynolds averaging (the so-called RANS approach), and so in this case averaging is simultaneously carried out over fluctuations due to turbulence and over those due to individual bubble motion. Even in Large Eddy Simulations (LES), the very large scale of the reactor relative to bubble size means that sub-grid scale averaging occurs over both turbulence and bubble-related fluctuations. These fluctuations are coupled, in that bubble motion generates turbulence directly at a scale comparable to the bubble size, that is, so-called bubble-induced turbulence.

At this point it is important to distinguish between such bubble-induced turbulence and turbulence generated by decay of large-scale mean flows driven by bubbles. As an example of the latter, bubbles concentrated into a bubble plume can generate very strong upward flow, and the resulting shear generates turbulence through the conventional instability mechanism.

It is also important to distinguish bubble-generated turbulence from turbulence modulation caused by particles; this latter effect is generally understood to mean the damping of turbulence that arises from drag between particles by turbulence eddies. By contrast,

bubble-generated turbulence arises from the disturbance to liquid streamlines resulting from the movement of liquid around bubbles. Crowe (2000) presented data that indicates that turbulence enhancement occurs for large particles/bubbles, whereas damping occurs for small particles/bubbles. This paper deals with the enhancement effect, and focuses on bubbles, but most of the results would also be applicable to large particles.

Bubble-generated turbulence has been the subject of several theoretical studies, but no generally accepted formulation suitable for the multi-fluid model has yet been developed. Furthermore, experimental studies of the phenomena are few because of the difficulty of isolating the effect from the multitude of other related ones. The approach taken is usually a variant of that pioneered by Johansen and Boysen (1988), in which a theoretical expression for energy generation is modified by means of a multiplicative coefficient, which is determined by comparison of simulation results with experiment.

The theoretical approaches that have been used to account for bubble induced turbulence are reviewed briefly in the next section. The benefits and drawbacks of each approach will be discussed. Then, a simple CFD simulation for flow around a single bubble is discussed, in order to better understand the assumptions behind these theoretical approaches.

THEORETICAL APPROACHES TO BUBBLE-INDUCED TURBULENCE

Bubble-induced eddy viscosity

The first estimate of the shear stress associated with bubble motion was by Sato and Sekoguchi (1975), who assumed that the total shear stress, τ , could be considered to be the sum of three components: that due to liquid viscosity, that due to momentum exchange resulting from conventional turbulence, and that due to momentum exchange resulting from bubble agitation:

$$\tau = \rho_l \alpha_g (\nu + \nu_t + \nu_{BIT}) \frac{d\bar{u}}{dy} \quad (1)$$

where ρ_l is the liquid density, α_g is void fraction, ν is kinematic viscosity, and ν_t is turbulent eddy viscosity. A two-dimensional configuration was analyzed in which \bar{u} is the mean velocity perpendicular to the y direction. To evaluate the “bubble induced eddy viscosity”, ν_{BIT} , they considered the liquid velocity fluctuations associated with flow past a bubble (assuming two-dimensional inviscid flow), as illustrated in Fig. 1. The fluctuations are the difference between velocities indicated in Fig. 1, and velocities in the flow without a bubble (or cylinder in 2D). They then averaged these fluctuations over a volume containing many such bubbles, to obtain:

$$\nu_{BIT} = \kappa \alpha d_b U_b, \quad (2)$$

where κ is an empirical constant, α is gas void fraction, and d_b and U_b are average values of bubble diameter and relative velocity (or bubble slip velocity). Sato *et al.* (1981) recommend a value of 0.6 for κ based on

comparison with experimental data. They also point out that Eqn (1) is just a Prandtl mixing length expression for eddy viscosity in a wake behind a solid body based on a mixing length and velocity deficit.

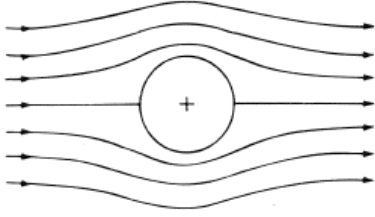


Figure 1: Streamlines for inviscid flow over a cylinder.

Turbulent stress due to bubble disturbances

Arnold *et al* (1989) carried out a similar but more rigorous analysis for the turbulent stresses generated by bubble-induced velocity fluctuations. Their analysis was also based on inviscid flow, though in three dimensions (i.e. around spheres). Because they take a more rigorous approach to the averaging procedure, they obtain a much more complex expression for the tensor stress, \mathbf{T} , due to bubble-related fluctuations:

$$\mathbf{T} = a_2 \mathbf{I} + b_2 (\mathbf{U}_g - \mathbf{U}_l)(\mathbf{U}_g - \mathbf{U}_l) + \mathbf{T}^S \quad (3)$$

plus terms in the gradient of the slip velocity, which can be neglected if the bubble size is locally uniform, as is usually the case. Here \mathbf{I} is the identity tensor, and \mathbf{U}_g and \mathbf{U}_l are averaged gas and liquid phase velocities respectively. The coefficients were found to be:

$$a_2 = \frac{3}{20} \rho_l \alpha_g |\mathbf{U}_g - \mathbf{U}_l|^2 \quad (4)$$

$$b_2 = \frac{1}{20} \rho_l \alpha_g \quad (5)$$

The last term in Eqn. (3), \mathbf{T}^S , is a second order function of gradients of mean flow velocity, and is proportional to $agdb^2$. The authors argue that this implies that the effective eddy viscosity is also predicted to be proportional to $agdb^2$, and to mean velocity gradient. For Stokes flow, $U_b \propto db$, so it could be argued that the eddy viscosity should be of a similar form to the Sato and Sekoguchi [3] expression, eq.(1), except for the presence of the factor dependent on velocity gradient.

It is important to understand that Sato and Sekoguchi (1975) and Arnold *et al* (1989) (as well as various authors who have followed this approach such as Nigmatulin (1979)) consider the velocity deviations associated with the flow of liquid around the sphere to be turbulence. Now the assumption of irrotational flow around a sphere, as used by these authors implies no dissipation. For a single isolated bubble, the upstream and downstream flows are (mirror image) symmetrical in this model, so that while the liquid is associated with velocity deviations as it passes the sphere (or as a bubble moves upward through liquid), the energy associated with these deviations is completely recoverable. Consequently, these velocity deviations should not be considered to be turbulence in the true sense. A rising bubble “carries” these velocity deviations with it as it rises, so there is no

source of turbulence energy and no dissipation. If these deviations are indeed considered to be a form of pseudo “turbulence energy”, the value of this energy is constant: there is no net source or sink as bubbles rise.

If the flow is strictly inviscid, then there can be no “eddy viscosity” associated with the bubble-generated velocity deviations for a single isolated bubble. As a bubble rises, liquid elements will oscillate as a result of these deviations, but will then return to the original locations – there will be no diffusion of fluid concentrations or momentum, and hence zero effective eddy viscosity.

We argue here that even in less ideal flows where the inviscid assumption is relaxed, a component of the fluctuation energy associated with bubble rise will be recoverable in the sense of inviscid flow, and should not be counted as bubble-induced turbulence. We use the term “recoverable energy” to mean the pseudo-turbulence component of the fluctuation energy that is not dissipated.

Thus the fluctuations associated with bubble motion in a real liquid (with viscosity) can be considered to consist of two components. The first is the deformational motion of streamlines around the bubble that can be predicted for inviscid flow similar to that shown in Fig. 1. As mentioned above, the kinetic energy of this component is constant, and there is no source or sink. The second component is the motion within the wake. Unlike the first component these fluctuations are indeed dissipated, and so are likely to resemble turbulence.

Since the turbulence kinetic energy is $k = \frac{1}{2} \overline{u'_i u'_i}$, where u'_i is the i -th component of liquid phase fluctuation velocity and the summation convention applies, the Arnold *et al* (1989) expression, eqs.(4) and (5), implies that the kinetic energy of the disturbed motion around bubbles (the pseudo-turbulence) is:

$$k_{BI} = \frac{1}{4} \alpha_g |\mathbf{U}_g - \mathbf{U}_l|^2 \quad (6)$$

Lopez de Bertodano *et al* (1994) argued that since Eqn (6) was based on inviscid flow for which the virtual mass coefficient, C_{vm} , is $\frac{1}{2}$, and the turbulence energy relates to the volume in the wake, the equation can be written more generally as:

$$k_{BI} = \frac{1}{2} \alpha_g C_{vm} |\mathbf{U}_g - \mathbf{U}_l|^2 \quad (7)$$

They have used a CFD model incorporating the Sato *et al* (1981) bubble-induced eddy viscosity and Eqn (7) to simulate bubbly pipe flow, and have then compared the results with detailed measurements of velocity, turbulence and void fraction. Note that Eqn (7) was not used in determining eddy viscosity, but was needed to determine the total mean fluctuation in velocity (or equivalently the components of normal stress) for comparison with data. The best agreement is generally found for $C_{vm} = 2$. This value is consistent with theoretical calculations by Lance and Bataille (1991) for oblate bubbles moving in helical paths, which yield values between 1.2 and 3.4.

Extending the argument given by Lopez de Bertodano *et al* (1994), the turbulence energy in the wake component could be obtained by subtracting the pseudo-turbulence component from total energy as estimated from the virtual mass, in other words:

$$k_{\text{BI}} = \frac{1}{2} \alpha_g (C_{\text{vm}} - 0.5) |\mathbf{U}_g - \mathbf{U}_l|^2. \quad (8)$$

They also argue that their comparisons between CFD simulation and experiment suggests that $C_{\text{vm}} = 2$ for bubbly flow in a pipe.

Lance and Bataille (1991) use a different argument. They roughly estimate the wake contribution to the kinetic energy from the dissipation rate, which is a fraction of the work performed by the drag force experienced by the bubbles,

$$\varepsilon_w \sim \alpha_g C_d |\mathbf{U}_g - \mathbf{U}_l|^3 / D. \quad (9)$$

where C_d is the drag coefficient and D is the bubble diameter, where the tilde here has the meaning approximately equal to within a factor of order unity. They then assume that the velocity fluctuations associated with this dissipation have a length scale ℓ_w , then the r.m.s. value of the fluctuations satisfies

$$u'_w{}^3 / \ell_w \sim \alpha_g C_d |\mathbf{U}_g - \mathbf{U}_l|^3 / D. \quad (10)$$

Lance and Bataille (1991) argue that Eqn (10) implies that the energy associated with turbulence production in the wakes should vary as $\alpha_g{}^{2/3}$. This is different from the normal linear assumption.

Lance and Bataille (1991) appear to have understood the point we make that a fraction of the fluctuation energy associated with bubble rise is recoverable and does not contribute to real turbulence. They mention both “inviscid pseudo-turbulent contributions” and “the turbulent fluctuations produced by the wakes of the bubbles”, but the descriptions are not precise, and in later experimental work, the distinction is lost and the term “pseudo-turbulence” has become synonymous with bubble-induced turbulence (Wijngaarden, 1998; Hosokawa and Tomiyama, 2013).

The experimental LDA data collected by Lance and Bataille (1991) imply that the turbulent fluctuations produced by the wakes of the bubbles contribute only a small part of the overall fluctuating kinetic energy, with the vast majority contributed by the pseudo-turbulence. This of course means that it is extremely difficult (if not impossible) to determine an expression for bubble-induced turbulence from such experimental measurements. For the same reason, it would difficult to determine an expression for bubble-induced turbulence from direct numerical simulation of a bubbly flow. One possible alternative approach would be to numerically study the situation of flow around a single bubble, where it may be easier to separate the contributions of pseudo-turbulence and wake turbulence. This is the approach followed below.

Generation rate of turbulence energy

Since a two-equation RANS model such as k - ε is often used in industrial CFD modelling, it is natural to seek to incorporate bubble-induced turbulence into this formalism. The approach has been to determine source terms for the k and ε equations to characterize the bubble effect.

The expression usually used for the rate of generation of turbulence energy originates from analysis by Besnard and Harlow (1988) and Kataoka and Serizawa (1989) of the averaged two-phase Navier-Stokes equations. They identified the fluctuations generated by the dispersed phase as turbulence. The source term for this turbulence was shown to be, under certain assumptions, to the product difference between the mean velocities of the two phases and the drag force:

$$S_k = \mathbf{F}_D \bullet (\mathbf{U}_g - \mathbf{U}_l) \quad (11)$$

As argued above, the velocity fluctuations generated by bubbles include both pseudo-turbulence as well as true turbulence, so the suitability of this formula is suspect. Nonetheless, many researchers have used it as the source term describing bubble-induced turbulence in RANS simulations of bubbly flow, though generally with an empirically determined multiplying factor (e.g., Rzehak and Krepper, 2013; Feng *et al.*, 2015). Unfortunately, the value of the empirical factor is found to vary over a very wide range (two orders of magnitude) depending on the data used, and this limits the predictive value of the formula (Schwarz, 2015).

As discussed by Schwarz (2015) and Rzehak and Krepper (2013), the source term for ε is even more uncertain than that for k .

CFD MODEL OF FLOW PAST A SINGLE BUBBLE

CFD model formulation

A CFD model of liquid flow past a single bubble is developed and analysed to determine the strength of wake turbulence. The model is transformed to a frame of reference in which the bubble is stationary: this should be a reliable approach except in cases where a substantial spiralling motion occurs as the bubble rises.

The bubble is taken to be spherical, as would be the case for high surface tension. The simulations for spherical bubbles are useful as a base case, with which turbulence generation by deformed bubbles can later be compared.

Bubble diameter is taken to be 5 mm, and the rise velocity of the bubble is 0.2 m/s. The density and viscosity of the liquid are taken to be those of water. Simulations are run for both mobile and immobile bubble interface, by applying respectively free-slip and no-slip boundary conditions.

The CFD model is a transient Reynolds Averaged Navier-Stokes (RANS) model applying the SST turbulence model equations.

The inlet condition is taken to be constant velocity, and the outlet condition is set to a so-called “outlet”, in which pressure is uniform and the streamwise derivative of convected quantities is zero. The computational domain is taken to be a cylinder, with free-slip wall conditions sufficiently far from the sphere that they should not appreciably affect the flow (namely at 10 bubble diameters).

The flow equations are solved using ANSYS CFX.

Model results (immobile interface)

The flowfield computed by the CFD model for immobile interface is illustrated in Figure 2 on a plane through the centre of the bubble. The entire domain is larger than that shown, but only the flowfield in the immediate vicinity of the bubble is of interest. There is clearly some asymmetry between upstream and downstream flows, which indicates the effect of viscosity. The computation is transient, but the computed Reynolds averaged flow is almost steady, with only a slight oscillation in the wake. Vortex shedding is expected to start for Reynolds number around 300 (Wu and Faeth, 1994) whereas the Re for the computed case is 1000. It is likely that the application of a turbulence model delays the onset of vortex shedding, and an LES or DNS simulation would undoubtedly give a more accurate prediction of the transition. However, the calculation and interpretation of a source of turbulence becomes more difficult for the results of such simulations. LES simulations will be analysed in the future.

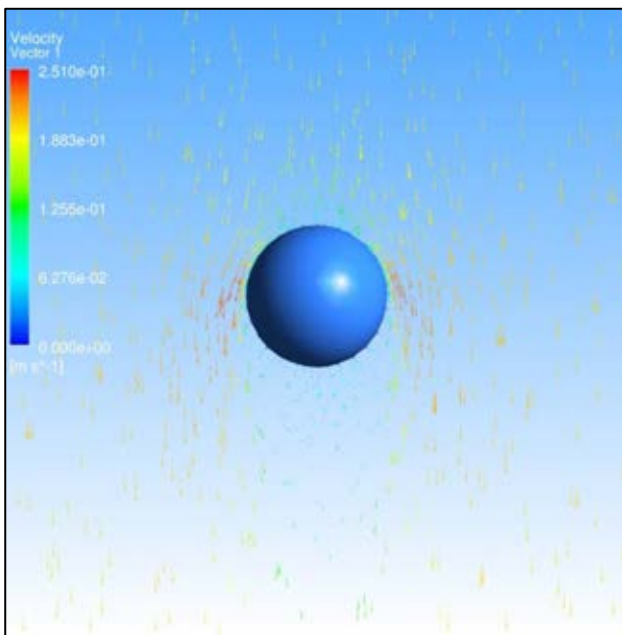


Figure 2: Computed flowfield past the spherical bubble (immobile interface). Colour indicates speed (m/s).

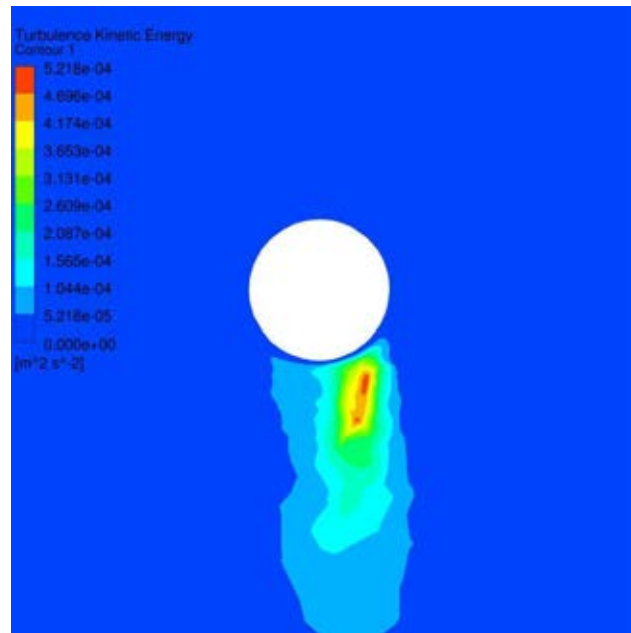


Figure 3: Contours of turbulence kinetic energy (m^2s^{-2}) for the computed flow past spherical bubble (immobile interface).
Maximum value: $5.22 \times 10^{-4} \text{ m}^2\text{s}^{-2}$

Figure 3 plots contours of turbulence kinetic energy for the computed flow past the immobile interface spherical bubble, and Figure 4 plots contours of the turbulence frequency. The spatial distribution of the generation term for turbulence energy is plotted in Figure 5.

It should be mentioned that the standard $k-\varepsilon$ turbulence model is not appropriate for this flow situation. Such a model predicts relatively high levels of turbulence generation in the boundary layer around the bubble, including the leading surface. The SST model is known to better capture flow in such boundary layers, and in fact, predicts a laminar boundary layer in this particular case. Turbulence generation only occurs in the wake.

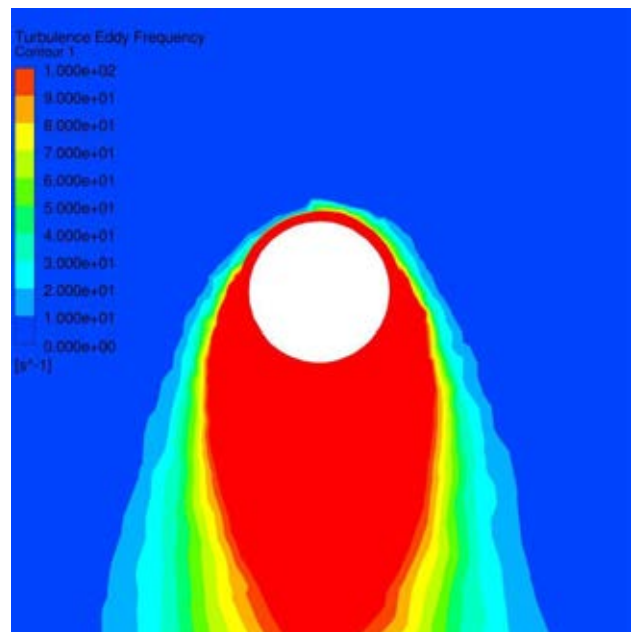


Figure 4: Contours of turbulence frequency (s^{-1}) for the computed flow past spherical bubble (immobile interface).
Maximum value: $1.0 \times 10^2 \text{ s}^{-1}$

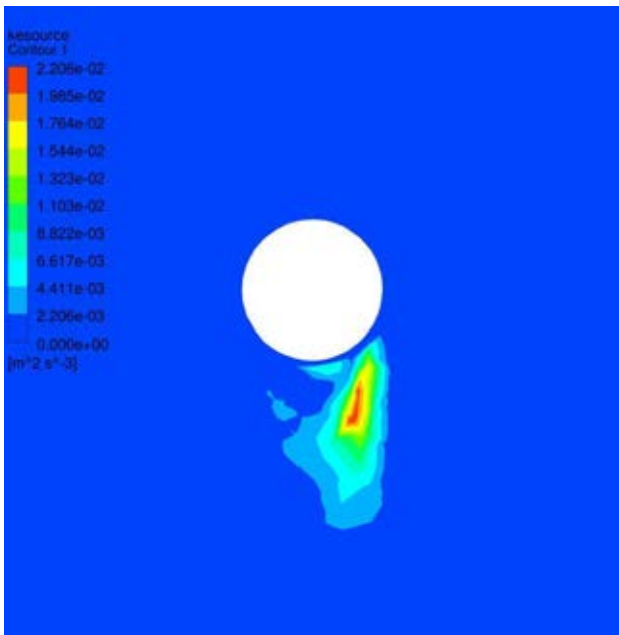


Figure 5: Contours of production rate of turbulence kinetic energy (m^2s^{-3}) for the computed flow past spherical bubble (immobile interface). Maximum value: $2.2 \times 10^{-2} \text{ m}^2\text{s}^{-3}$

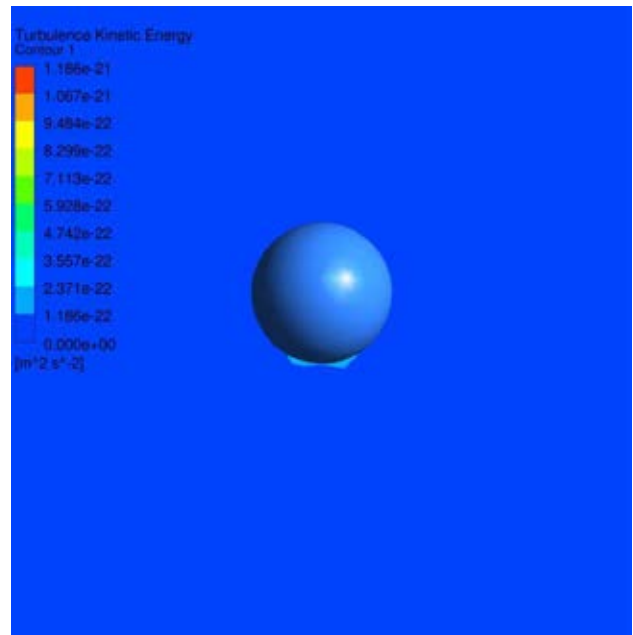


Figure 7: Contours of turbulence kinetic energy (m^2s^{-2}) for the computed flow past spherical bubble (mobile interface). Maximum value: $1.19 \times 10^{-21} \text{ m}^2\text{s}^{-2}$

Figs 3 and 5 indicate that the turbulence energy and generation rate are distributed asymmetrically at this instant of time. While there is some movement in these zones as time progresses, they continue to be asymmetric. This is related to slight asymmetry in the computed flowfield which may be caused by an intrinsically unstable flow, perhaps aggravated by asymmetries in the computational mesh.

The total source of turbulence kinetic energy integrated over the entire domain is $1.03 \times 10^{-6} \text{ kgm}^2\text{s}^{-3}$.

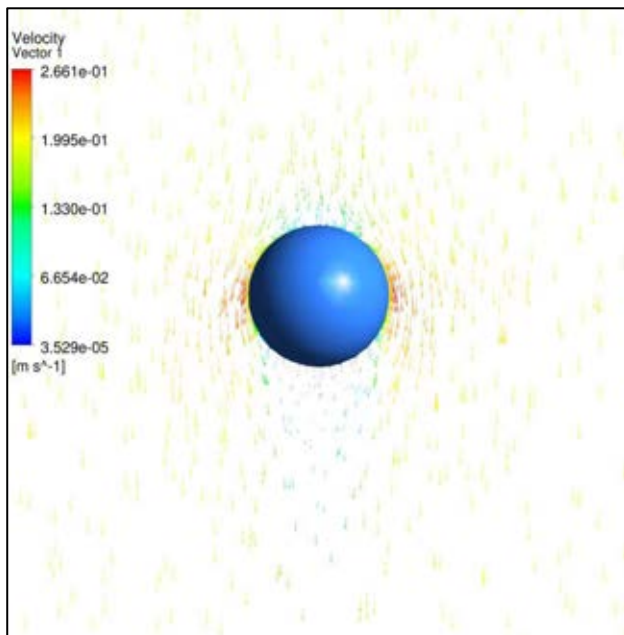


Figure 6: Computed flowfield past the spherical bubble (mobile interface). Colour indicates speed (m/s).

Model results (mobile interface)

The flowfield computed by the CFD model for a mobile interface is illustrated in Figure 6 on a plane through the centre of the bubble. The lateral and longitudinal extent of the wake region is reduced relative to that formed for an immobile interface (Figure 2).

Figure 7 plots contours of turbulence kinetic energy for the computed flow past the mobile interface spherical bubble, and Figure 8 plots contours of the turbulence frequency. The spatial distribution of the generation term for turbulence energy is plotted in Figure 9. These plots clearly indicate that the generation of turbulence energy in the wake is insignificant for a mobile interface when the bubble size is 5 mm.

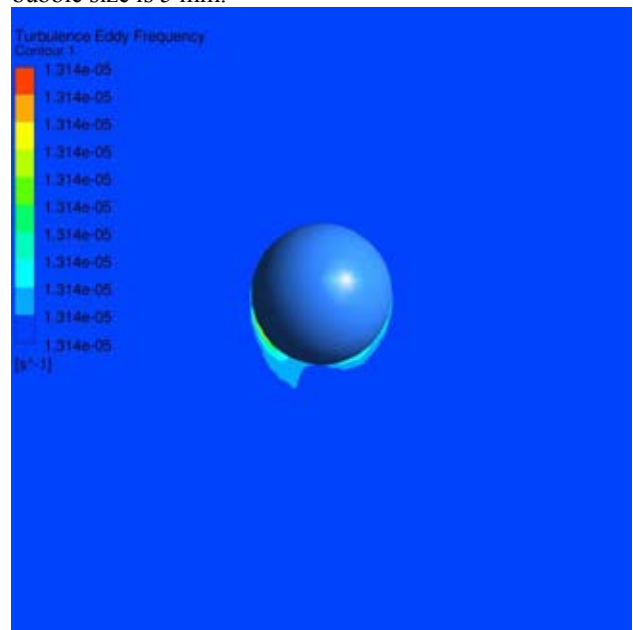


Figure 8: Contours of turbulence frequency (s^{-1}) for the computed flow past spherical bubble (mobile interface). Maximum value: $1.31 \times 10^{-5} \text{ s}^{-1}$

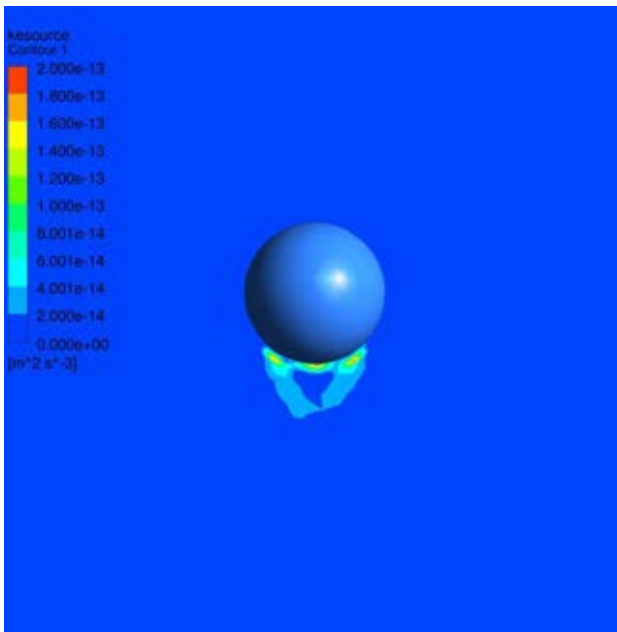


Figure 9: Contours of production rate of turbulence kinetic energy (m^2s^{-3}) for the computed flow past spherical bubble (mobile interface). Maximum value: $2.0 \times 10^{-13} \text{m}^2\text{s}^{-3}$

DISCUSSION

As mentioned above, according to the turbulence model, the total source of turbulence kinetic energy integrated over the entire domain for the immobile interface bubble of size 5 mm is $1.03 \times 10^{-6} \text{kgm}^2\text{s}^{-3}$. One would expect that this source term would be one component of the source term for turbulence energy generated by the bubble.

The mean flow shown in Figure 2 consists of two components: the flow attached to the bubble whose energy is recoverable, and the energy in the wake which will contribute to the turbulence energy generated by the bubble. There is no well-defined procedure for separating these components, but we assume that the energy at two diameters downstream can be taken to be the wake energy. In this case (immobile interface bubble of size 5 mm) we find the energy source to be $1.26 \times 10^{-6} \text{kgm}^2\text{s}^{-3}$.

Now the theoretical argument encapsulated in Eqn (11) means that the turbulence energy generation should be given by the product of drag and slip velocity. If we assume that in steady state the drag force equals the buoyancy force on the bubble, then we can readily calculate the theoretical generation rate to be $1.28 \times 10^{-4} \text{kgm}^2\text{s}^{-3}$. This is substantially greater than the turbulence energy generation rate predicted by the CFD model. This difference can be explained by the fact that the product of drag and slip velocity is the total energy dissipation, but only part of that occurs through turbulence generation. The Reynolds number for the situation modelled is relatively low, so one would expect that a large fraction of the energy dissipation could occur directly through viscous forces, rather than indirectly via turbulence generation. After all, for laminar flow, the entire energy dissipation is directly through viscous forces. Thus, it appears that the theoretical formula often used as a basis for estimating bubble-induced turbulence

generation is not applicable for low Reynolds number (i.e. small bubbles).

Simulations are presently being carried out for larger bubbles, where it might be expected that higher rates of turbulence energy generation occurs, and the theoretical formula may better predict the generation rate. However, bubbles of size 1 cm and larger (at least in water) are subject to substantial distortion as they rise, so the simplified method used here would not be appropriate unless a greater surface tension was assumed.

The theoretical formula is even less applicable for the case of mobile interface. As seen in Figures 7-9, the generation rate of turbulence in this case is predicted to be negligible for the SST turbulence model. In effect, this flow is entirely viscous. Real bubbles will always have a certain degree of immobility, and in the case of water with surfactants, the interfaces can be substantially immobile. Larger bubbles with mobile interfaces will be subject to deformation, which will introduce additional sources of turbulence generation.

The equivalent values of turbulence dissipation rate can be computed for the SST model from turbulence energy and frequency. For the immobile case, the total dissipation rate is calculated from the CFD simulation results to be $1.005 \times 10^{-6} \text{kgm}^2\text{s}^{-3}$. It is noteworthy that this value is only slightly smaller than the total turbulence energy generation rate. That is to say, almost all the turbulence energy generated is dissipated locally, within the wake attached to the bubble. Very little energy is transported away from the bubble into the bulk flow.

CONCLUSION

Models proposed to account for bubble-induced turbulence in two-fluid Reynolds-averaged (RANS) simulations of bubbly flow have been reviewed, and the assumptions underlying the models have been critically assessed.

1. There has been a neglect of the difference between so-called “false turbulence” (velocity fluctuations attached to the bubble whose energy is recoverable) and true turbulence (fluctuations not attached to the bubble, which can diffuse into the flow as modelled by the transport equation for k).
2. The estimates of bubble-generated turbulence by Arnold *et al* (1989) and others are entirely of the false turbulence, since they assume inviscid flow, in which the “fluctuation energy” is entirely recovered.
3. Consideration of the false turbulence component of the fluctuations raises very real issues of definition of bubble induced turbulence, and also implies that direct measurement of real bubble induced turbulence (using LDA for example) will be very problematic.
4. Simulation of the rise of a 5 mm bubble underlines how most of the fluctuation energy is recoverable. Most of the energy dissipation is

through direct viscous dissipation, rather than indirectly via generation of true turbulence.

5. Generation of true turbulence will undoubtedly be greater for larger bubbles and intrinsically unsteady bubble rise, but it is unclear whether the conventional theoretical formula for generation rate will be applicable, given that it does not appear to apply in the case of 5 mm bubbles.

REFERENCES

- ARNOLD, G.S., DREW, D.A. and LAHEY, R.T., (1989), "Derivation of constitutive equations for interfacial force and Reynolds stress for a suspension of spheres using ensemble averaging", *Chem. Eng. Comm.*, **86**, 43–54.
- BESNARD, D.C. and HARLOW, F.H., (1988), "Turbulence in multiphase flow". *Int. J. Multiphase Flow*, **14**, 679–699.
- CROWE, C.T., (2000), "On models for turbulence modulation in fluid-particle flows", *Int. J. Multiphase Flow*, **26**, 719–727.
- FENG, Y.Q., SCHWARZ, M.P., YANG, W. and COOKSEY, M., (2015), "Two-phase CFD model of the bubble-driven flow in the molten electrolyte layer of a Hall-Héroult aluminum cell", *Metall. Mat. Trans. B*, **46**, 1959–1981.
- HOSOKAWA, S., and TOMIYAMA, A., (2013), "Bubble-induced pseudo turbulence in laminar pipe flows", *Inter. J. Heat and Fluid Flow*, **40**, 97–105.
- JOHANSEN, S.T. and BOYSAN, F., (1988), "Fluid Dynamics in Bubble Stirred Ladles; Part II: Mathematical Modelling", *Met. Trans. B*, **19**, 755–764.
- KATAOKA, I. and SERIZAWA, A., (1989), "Basic equations of turbulence in gas-liquid two-phase flow". *Int. J. Multiphase Flow*, **15**, 843–855.
- LANCE, M. and BATAILLE, J., (1991), "Turbulence in the liquid phase of a uniform bubbly air-water flow", *J. Fluid Mech.*, **222**, 95–118.
- LOPEZ DE BERTODANO, M., LAHEY, R.T. and JONES, O.C., (1994), "Development of a k-ε model for bubbly two-phase flow", *J. Fluids Eng. Trans ASME*, **116**, 128–134.
- NIGMATULIN, R.I., (1979), "Spatial averaging in the mechanics of heterogeneous and dispersed systems", *Int. J. Multiphase Flow*, **5**, 353–385.
- RZEHAK, R. and KREPPER, E., (2013), "CFD modeling of bubble-induced turbulence". *Int. J. Multiphase Flow*, **55**, 138–155.
- SATO, Y. and SEKOGUCHI, K., (1975), "Liquid velocity distribution in two-phase bubbly flow", *Int. J. Multiphase Flow*, **2**, 79–95.
- SATO, Y., SADATOMI, M. and SEKOGUCHI, K., (1981), "Momentum and heat transfer in two-phase bubble flow", *Int. J. Multiphase Flow*, **7**, 167–177.
- SCHWARZ, M.P., (2015), "Bubble induced turbulence in two-fluid simulation of bubbly flow", *26th International Symposium on Transport Phenomena*, Leoben, Austria, 27 September–1 October 2015.
- SCHWARZ, M.P. and FENG, Y.Q., (2015), "Pragmatic CFD modelling approaches to complex multiphase processes", *Progress in Applied CFD*, J.E. Olsen and S.T. Johansen Eds, SINTEF, 25–38.
- SPALDING, D.B., (1981), "A general purpose computer program for multi-dimensional one- and two-phase flow", *Mathematics and Computers in Simulation*, **23**, 267–276.
- VAN WIJNGAARDEN, L., (1998), "On Pseudo Turbulence", *Theoret. Comput. Fluid Dynamics*, **10**, 449–458.
- WU, J.-S. and FAETH, G.M., (1994), "Sphere wakes at moderate Reynolds numbers in a turbulent environment", *AIAA J.*, **32**, 535–541.